Long-range function of secreted small nucleolar RNAs that direct 2′-*O*-methylation

Jamie M. Rimer[‡], Jiyeon Lee[‡], Christopher L. Holley[‡], Robert J. Crowder[‡], Delphine L. Chen[‡§], Phyllis I. Hanson[¶], Daniel S. Ory[‡], and ⓘ Jean E. Schaffer[‡1]

From the [‡]Department of Medicine, [§]Mallinckrodt Institute of Radiology, and [¶]Department of Cell Biology and Physiology, Washington University School of Medicine, St. Louis, Missouri 63110

Edited by Karin Musier-Forsyth

Small nucleolar RNAs (snoRNAs) are noncoding RNAs that guide chemical modifications of structural RNAs. Whereas snoRNAs primarily localize in the nucleolus, where their canonical function is to target nascent ribosomal RNAs for 2′-*O*-methylation, recent studies provide evidence that snoRNAs traffic out of the nucleus. Furthermore, RNA-Seq data indicate that extracellular vesicles released from cells contain snoRNAs. However, it is not known whether snoRNA secretion is regulated or whether secreted snoRNAs are functional. Here, we show that inflammation stimulates secretion of *Rpl13a* snoRNAs U32a (SNORD32a), U33 (SNORD33), U34 (SNORD34), and U35a (SNORD35a) from cultured macrophages, in mice, and in human subjects. Secreted snoRNAs co-fractionate with extracellular vesicles and are taken up by recipient cells. In a murine parabiosis model, we demonstrate that snoRNAs travel through the circulation to function in distant tissues. These findings support a previously unappreciated link between inflammation and snoRNA secretion in mice and humans and uncover a potential role for secreted snoRNAs in cell–cell communication.

The nearly 400 snoRNAs[2] encoded within mammalian genomes function in 2′-*O*-methylation, pseudouridylation, or processing of other cellular RNAs (1, 2). Typically, snoRNAs direct these modifications on rRNAs and small nuclear RNAs, with specificity in targeting achieved by base pairing between the snoRNA antisense elements and their targets. Most mammalian snoRNAs are encoded within introns of host genes and are released from intron lariats during splicing by debranching

and exonucleolytic cleavage (3). A small number of snoRNAs are independently transcribed by RNA polymerase II, with an m^7G cap structure that becomes hypermethylated and a short 3′ extension that is cleaved (4). The vast majority of cellular snoRNAs localize with their substrates in the nucleus. Intronic snoRNAs are produced within the nucleoplasm, complexed with proteins, and transported to the nucleoli, where they are well positioned to encounter nascent rRNA substrates (5). By contrast, independently transcribed snoRNAs traffic to the cytoplasm during their biogenesis and are efficiently retrieved to the nucleus (6, 7).

A number of studies suggest that snoRNA localization to the nucleus is dynamic and regulated. In the setting of serum starvation of fibroblasts, biogenesis of snoRNA U3 increases, and abundance of U3 in the cytoplasm increases (8). Our own work has demonstrated that the snoRNAs encoded in the *Rpl13a* locus, U32a (SNORD32a), U33 (SNORD33), U34 (SNORD34), and U35a (SNORD35a), are essential for the cell death response to metabolic stress and accumulate in the cytosol of fibroblasts and myoblasts in response to lipotoxic and oxidative stress (9). RNA-Seq studies from our laboratory provided evidence that box C/D snoRNAs as a class rapidly relocalize to the cytoplasm following treatment of cardiomyoblasts with doxorubicin, a known inducer of oxidative stress (10). This redistribution of snoRNAs depends on superoxide and NADPH oxidase activity and does not simply result from compromise of the nuclear compartment. We also recently found that nuclear export factor 3 (NXF3) regulates the trafficking of snoRNAs between the nucleus and cytosol (11). Importantly, regulated appearance of snoRNAs in the cytoplasm raises the possibility of novel functions for snoRNAs outside the nucleus.

Microarray and deep sequencing approaches have led to the discovery of small noncoding RNAs in the extracellular space. The most well studied of these species are miRNAs, which are found in plasma in small membrane-bound vesicles or exosomes and/or bound to lipoproteins (12, 13). The abundance of different miRNAs in plasma, serum, and urine tracks with a spectrum of neurological, cardiovascular, oncologic, metabolic, and hematological disorders, suggesting that miRNAs in the blood can serve as biomarkers for disease processes (14). The observations that miRNAs are transferred from donor to recipient cells in which they impact gene expression and biological functions indicate that miRNAs can play roles in cell–cell communication (13, 15, 16).
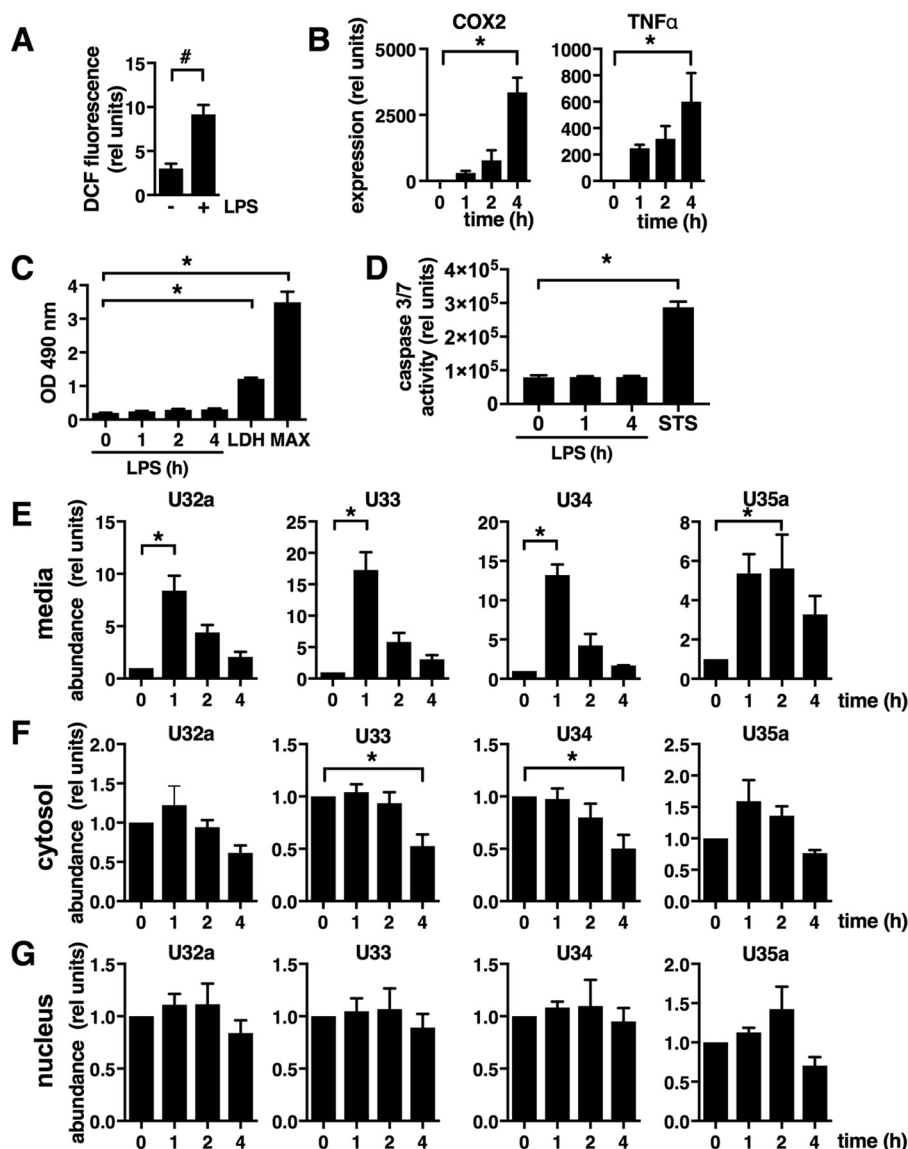
Figure 1. Macrophages secrete *Rpl13a* snoRNAs in response to lipopolysaccharide. Murine macrophages were treated with 50 ng/ml LPS. *A*, ROS quantified after 8 h by DCF staining. *B*, qRT-PCR quantification of *COX2* and *TNFα* gene expression relative (*rel*) to *Rplp0* at the indicated times. *C*, LDH release following treatment with 50 ng/ml LPS for the indicated time. LDH-positive control and freeze-thaw lysis (*MAX*) are shown as controls. *D*, apoptosis quantified by a caspase 3/7 activity assay. Cells were treated with 1.5 μM staurosporine (*STS*) for 4 h as a positive control. *E*, qRT-PCR of U32a, U33, U34, and U35a snoRNAs in medium relative to *C. elegans* miR39 spike-in. *F* and *G*, qRT-PCR quantification of *Rpl13a* snoRNAs U32a, U33, U34, and U35a relative to *Rplp0* in cytosolic (*F*) and nuclear (*G*) fractions. Results are mean ± S.E. (*error bars*) for $n \geq 3$ per condition. $p < 0.05$, using Student's *t* test (#) or ANOVA with Dunnett's multiple-comparison test (*).

RNA-Seq has also revealed the presence of snoRNAs in the medium of cultured cells (17–19) and in human plasma exosomes (20, 21). However, it is unclear whether secretion of this class of noncoding RNAs is regulated, and in contrast to miRNAs, their potential to function in non-cell-autonomous roles is unknown. The present study was undertaken to further characterize the extracellular trafficking of the four intronic box C/D snoRNAs produced from the *Rpl13a* locus.

Results

Rpl13a snoRNAs accumulate in the culture medium of lipopolysaccharide (LPS)-stimulated macrophages

The *Rpl13a* snoRNAs U32a, U33, U34, and U35a accumulate outside the nucleus of fibroblasts and cardiomyoblasts in the setting of oxidative stress (9, 10, 22). To extend these findings to

another cell type in which oxidative stress plays a central role in pathophysiologically important responses, we treated bone marrow–derived macrophages with LPS, a stimulus known to induce reactive oxygen species and inflammatory gene expression (23). Following exposure of macrophages to LPS, intracellular reactive oxygen species are increased, as evidenced by enhanced 2',7'-dichlorodihydrofluorescein diacetate (DCF) staining (Fig. 1A) and expression of the well-characterized inflammatory response genes, cyclooxygenase 2 and tumor necrosis factor-α (*COX2* and *TNFα*; Fig. 1B). Stimulation with LPS did not cause loss of cellular integrity, as assessed by LDH release (Fig. 1C), or apoptosis, as assessed by caspase 3/7 activity (Fig. 1D). Using snoRNA-specific stem loop primers for reverse transcription with qPCR amplification for detection, we found that the *Rpl13a* snoRNAs rapidly increased in the
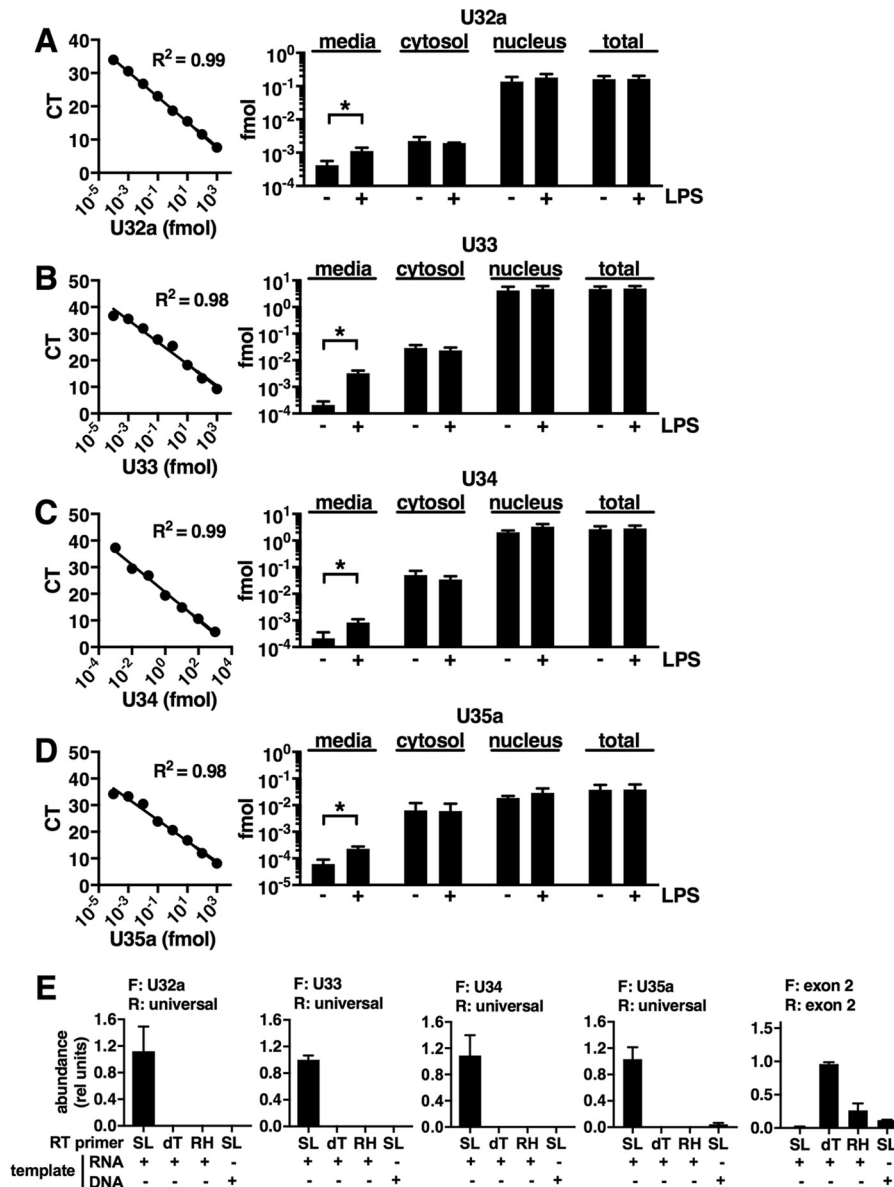
Figure 2. Detection of Rpl13a snoRNAs in medium is sensitive and specific. *A–D*, absolute abundance of *Rpl13a* snoRNAs. Standard curves display amplification of each purified *Rpl13a* snoRNA (*left*) and corresponding absolute quantification of each snoRNA in medium, cytosol, nucleus, and whole cell before and following treatment for 1 h with 50 ng/ml LPS (*right*) for U32a (*A*), U33 (*B*), U34 (*C*), and U35a (*D*). *E*, snoRNA-specific stem-loop (*SL*) primers for reverse transcription from RNA and DNA, compared with oligo(dT) priming (*dT*) and random hexamer priming (*RH*) from RNA. Shown is detection of snoRNA sequences by qPCR using the indicated snoRNA-specific forward primers and the exogenous universal reverse primer and detection of pre-mRNA and mRNA using forward and reverse primers designed within *Rpl13a* exon 2, which lies upstream of the snoRNAs in the transcript. Results are mean ± S.E. (*error bars*) for $n = 3$. $p < 0.05$, using Student's *t* test (*).

medium following 1 h of stimulation and were cleared over the subsequent 3 h (Fig. 1*E*). Increases in snoRNAs in the medium were not accompanied by increase in cytosolic or nuclear snoRNA abundance (Fig. 1, *F* and *G*). Absolute quantification of snoRNAs using standard curves for each species demonstrated that LPS-induced increases in snoRNAs in the medium are significant and specific, but small relative to nuclear and total cellular snoRNA abundance, pools that do not significantly change with treatment (Fig. 2, *A–D*). Control PCRs indicated that the target-specific stem-loop primed reverse transcription qPCR method detects mature snoRNAs, but not snoRNA sequences in DNA or pre-mRNA templates (Fig. 2*E*). These findings indicate that LPS induces macrophage snoRNA secretion. Rapid

clearance of the snoRNAs from the medium suggests they may be degraded, and decreases in cytosolic snoRNAs at 4 h (significant for U33 and U34 only) may reflect the cumulative export over several hours. In addition to the *Rpl13a* snoRNAs, LPS also stimulates the secretion of SNORD82, SNORD92, and SNORA73b (Fig. 3), suggesting that LPS broadly stimulates secretion of box C/D and box H/ACA snoRNAs.

Rpl13a snoRNAs are released with extracellular vesicles

A growing body of literature provides evidence that RNAs are released from cells in membrane-bound structures, generally referred to as extracellular vesicles (EVs) (24). Release of *Rpl13a* snoRNAs from LPS-stimulated macrophages was unaf-
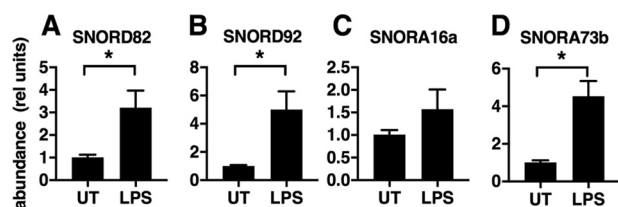
Figure 3. Macrophages secrete box C/D and box H/ACA snoRNAs in response to LPS. Macrophages were treated with 50 ng/ml LPS for 1 h. *A–D*, qRT-PCR of box C/D snoRNAs SNORD82 (*A*) and SNORD92 (*B*) and box H/ACA snoRNAs SNORA16a (*C*) and SNORA73b (*D*) in the medium. Results are mean ± S.E. (*error bars*) relative to *C. elegans* miR39 spike-in for *n* = 3. *p* < 0.05, using Student's *t* test (*).

fected by brefeldin A, suggesting that release of these RNAs did not require classical secretory pathways (Fig. 4, *A* and *B*). Appearance of *Rpl13a* snoRNAs in the medium was also stimulated by 2-hydroxypropyl-β-cyclodextrin and ionomycin, agents known to induce EV secretion though mechanisms that are distinct from LPS treatment (25, 26) and that do not lead to ROS generation (Fig. 4, *C* and *D*). Together, these observations suggested that release of *Rpl13a* snoRNAs into the medium might occur through EV secretion.

To determine whether snoRNAs in the medium are associated with EVs, we concentrated EVs from macrophage-conditioned medium following LPS treatment using either a commercial precipitation reagent that enriches for exosomes or differential centrifugation. Ultrastructural analysis of pellets isolated with both methods revealed membrane-bound structures with diameters of 70–200 nm (Fig. 5*A*), whereas these structures were absent from nonconditioned medium (not shown). In these quick-freeze deep-etch electron micrographs, either the true (outer) membrane surface or the smooth surface that results from fracturing through the two leaflets of the bilayer (p face) is visible at the perimeter of the vesicle. These data indicate that bone marrow–derived macrophages treated with LPS release EVs. Moreover, in EV-enriched fractions prepared by either method, *Rpl13a* snoRNAs were detected at baseline and increased following treatment of cells with LPS or ionomycin, indicating that macrophages constitutively release EV-associated snoRNAs but tightly regulate partitioning of snoRNAs for EV-mediated export in response to these stimuli (Fig. 5*B*). Recovery of EV-associated snoRNAs was more efficient following precipitation than ultracentrifugation, consistent with previous reports of higher yields from precipitation (27). EV preparations were enriched for the integral membrane proteins, flotillin and CD9, and relatively depleted for endoplasmic reticulum (calnexin) and nuclear (histone H3) markers (Fig. 5*C*). The absence of correlation between magnitude of stimulated EV-associated snoRNA secretion and EV-associated protein secretion between the two isolation methods and the lack of increase in EV-associated proteins between unstimulated and stimulated samples are observations that suggest snoRNA-containing EVs released upon LPS or ionomycin treatment represent a small fraction of the total secreted EVs.

To distinguish between co-fractionation and true association of *Rpl13a* snoRNAs with EVs, we separated EVs isolated by ultracentrifugation from potentially nonvesicular co-sedimenting components by floating the EVs into a continuous sucrose

gradient. Both *Rpl13a* snoRNAs and EV membrane protein markers were enriched at a density between 1.14 and 1.20 g/cm², the characteristic density for EVs (Fig. 6*A*). *Rpl13a* snoRNAs in these EVs were resistant to RNase treatment but degraded when treated with RNase in the presence of detergent (Fig. 6*B*), suggesting that the snoRNAs are protected by a membrane. Together, our findings support a model in which macrophages release EVs containing snoRNAs.

EV-associated Rpl13a snoRNAs are internalized by recipient cells

Secreted RNAs can impact the biology of target cells by engaging cell surface receptors or by uptake through endocytosis or macropinocytosis. To determine whether RNA from macrophage-derived EVs is incorporated into recipient cells, EVs were enriched from the medium of donor cells that had been metabolically labeled with ethynyl uridine and incubated for 45 min with unlabeled recipient cells. Following washing to remove surface-bound material, recipient cells were probed with an Alexa Fluor 594–linked click reagent. RNA from donor cell EVs was detected in the nucleus, where it co-localized with fibrillarin (Fig. 7*A*). The dye-only control indicates that any small amount of free dye that might remain after labeling and cleanup does not cause detectable nucleolar staining. In an alternate approach, RNA and lipids of isolated EVs were stained with Syto RNAselect and 1,1′-dioctadecyl-3,3,3′,3′-tetramethylindotricarbocyanine perchlorate (DiD), respectively, and incubated with recipient cells. In the recipient cells, labeled RNA was distributed throughout the cytoplasm and nucleus and concentrated in nuclear structures suggestive of nucleoli (*arrowheads*), a pattern that was distinct from background autofluorescence in the dye-only control (Fig. 7*B*). DiD was also transferred to recipient cells and was distributed in cytosolic punctae. Together, these findings indicate that both RNA and lipid constituents of EVs are transferred.

Approaches in which RNA is followed by a metabolic label or dye cannot formally distinguish between uptake of exogenous EV components and transfer of free label or dye that has partitioned into the EVs. To specifically assess whether secreted snoRNAs are taken up into recipient cells, we isolated cells from WT mice and from mice with germ line knockout of all four *Rpl13a* snoRNAs (KO) (28). KO mice are viable and fertile with no overt pathophysiological phenotype under standard housing and feeding conditions. However, pancreatic islets from these mice have decreased ROS tone, resistance to oxidative stress stimuli, and enhanced insulin secretion and mitochondrial proton leak.

WT and KO macrophages were co-cultured in a transwell apparatus that maintains the cells in separate compartments separated by a membrane with 1-μm pores. In this setting, medium and associated EVs were freely shared between the cells of different genotypes, but PCR analysis of DNA confirmed that cellular material was not transferred (Fig. 8*A*). *In situ* hybridization to detect snoRNA U33 revealed scattered nuclear puncta and larger areas of nuclear accumulation consistent with nucleoli in singly cultured WT cells (Fig. 8, *B* and *C*). Compared with KO macrophages that had been co-cultured with KO macrophages, KO macrophages co-cultured with WT
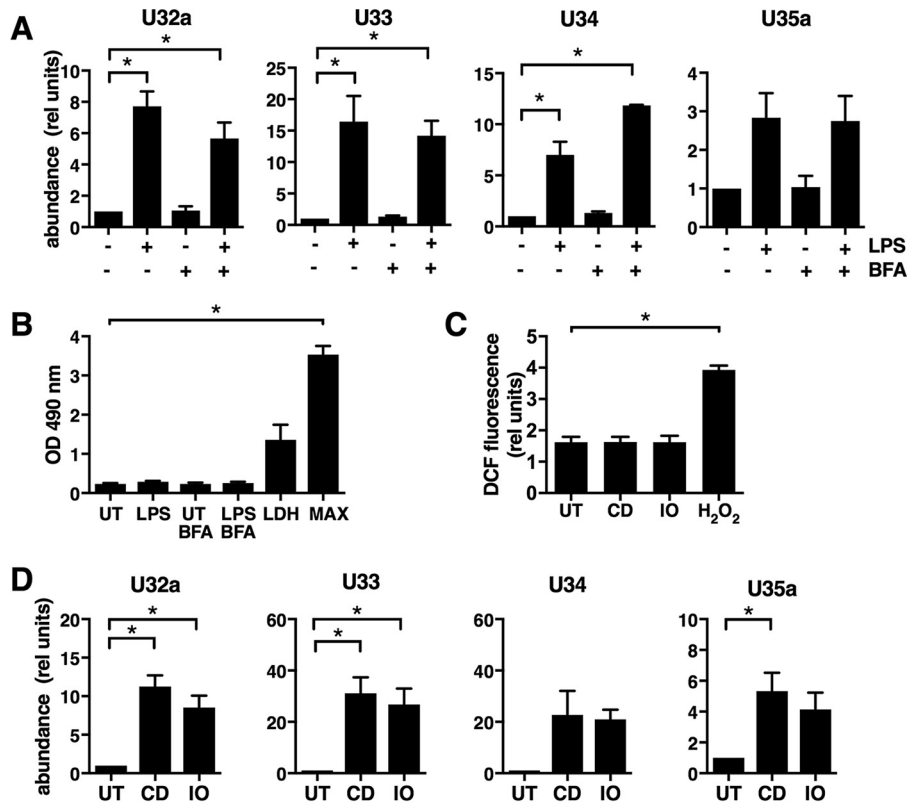
Figure 4. LPS stimulates nonclassical secretion of snoRNAs. *A* and *B*, macrophages were untreated (*UT*) or treated with 50 ng/ml LPS for 1 h in the absence or presence of 10 μg/ml BFA. *A*, qRT-PCR of snoRNAs U32a, U33, U34, and U35a in medium relative to *C. elegans* miR39 spike-in. *B*, LDH release as a measure of cell death. LDH-positive control and freeze-thaw lysis (*MAX*) are shown as controls. *C*, quantification of ROS by DCF staining and flow cytometric analysis following treatment with CD or IO. *D*, qRT-PCR of snoRNAs in medium from CD- or IO-treated cells. Results are means ± S.E. (*error bars*) for $n = 3$. *, $p < 0.05$ using ANOVA with Dunnett's multiple-comparison test.

macrophages demonstrated significantly increased nuclear punctae, consistent with transfer of U33. Whereas the signal for this single snoRNA species is small compared with the signal for total labeled RNA (Fig. 7), the co-culture approach (Fig. 8) provides further evidence of snoRNA transfer under more physiological conditions.

LPS increases Rpl13a snoRNAs in the serum of murine model and human volunteers

Because LPS triggers EV release of snoRNAs from cultured macrophages, we asked whether this inflammatory stimulus precipitated secretion of snoRNAs *in vivo* by treating mice with LPS. Compared with PBS-treated mice, animals that received LPS demonstrated a rapid increase in EV-associated *Rpl13a* snoRNAs in the serum over 4 h, concomitant with an increase in hepatic inflammatory gene expression (Fig. 9, *A* and *B*). We extended these findings by quantifying serum snoRNAs in healthy human volunteers undergoing intrabronchial instillation of LPS for a study of lung inflammation (29). Although the dose of LPS was small and delivered locally in the lungs, an increase in C-reactive protein, white blood cell count, and percentage of polymorphonuclear leukocytes 6 h following the procedure indicated the presence of systemic inflammation (Fig. 9*C*). Compared with pretreatment conditions, levels of U32a, U33, and U35a in serum EVs were significantly increased, and levels of U34 trended up (Fig. 9*D*). Thus, in mice and in humans, as we previously observed in cultured macrophages, LPS induces secretion of snoRNAs, most likely in EVs.

Secreted snoRNAs direct new 2′-O-methylation in vivo

To determine whether secreted snoRNAs can function in distant tissues *in vivo*, we employed a parabiosis model in which WT mice expressing GFP in all tissues were surgically joined to *Rpl13a* snoRNA KO mice (Fig. 10*A*). PCR analysis of DNA from tail blood of the parabionts revealed the presence of both the WT and KO alleles in the circulation of each parabiont by 1 week following surgery (Fig. 10*B*), consistent with reports of rapid development of shared circulation in this model (30). To test for the function of the *Rpl13a* snoRNAs, we utilized a qPCR-based method for detection of 2′-O-methylation of RNA, the modification that these snoRNAs direct on their canonical rRNA targets (31, 32). In this assay, the covalent modifications of the template cause reverse transcriptase to stall at low deoxyribonucleotide concentrations, such that larger amounts of qPCR product indicate less modification (Fig. 11*A*). This approach revealed the expected increases in amplification across *Rpl13a* snoRNA–directed 2′-O-methylation sites on the 18S and 28S rRNAs in KO compared with WT macrophages (Fig. 11*B*).

We applied this method for analysis of *Rpl13a* snoRNA–directed rRNA modifications to tissues harvested 3 weeks following surgery from KO and WT parabionts. Because new rRNA transcription correlates with cell replication (33) and 2′-O-methylation occurs on nascent rRNAs (34), we chose for study the intestinal epithelium, where cells turn over every 2–3 days (35). Liver tissue served as a negative control, because
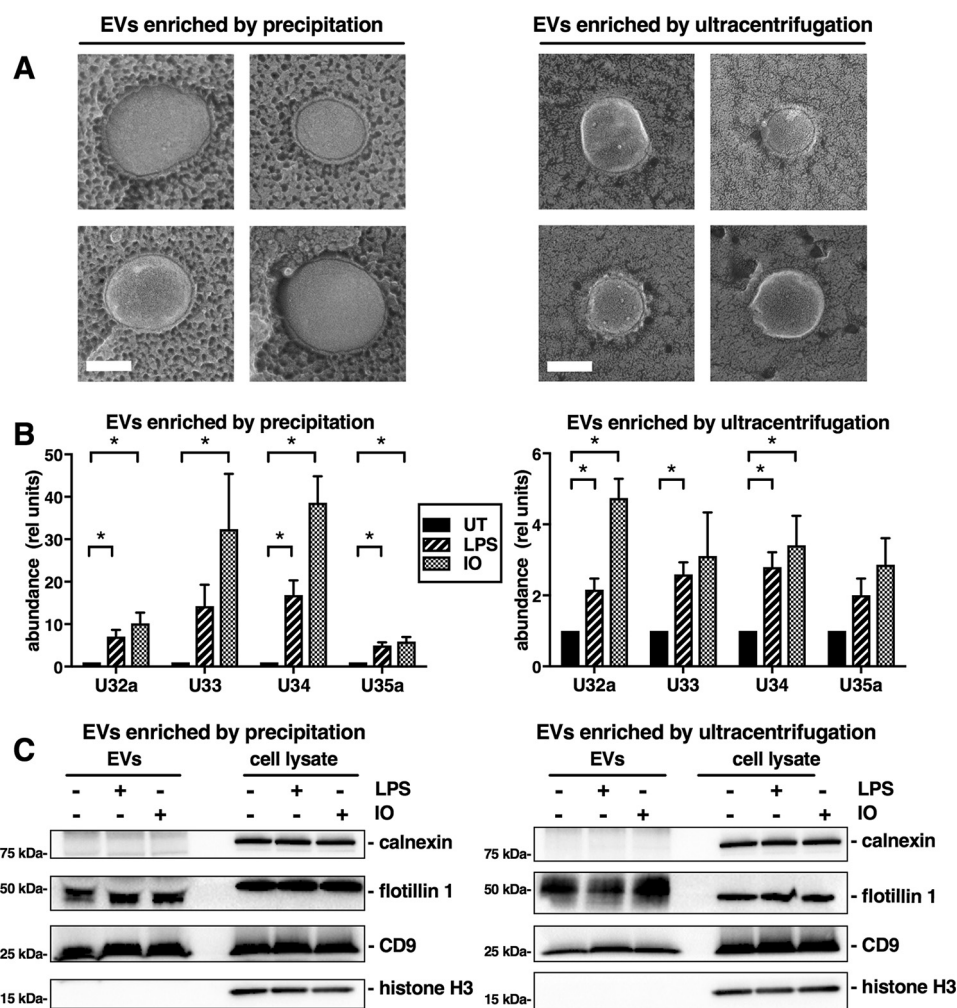
Figure 5. snoRNAs are associated with EV fraction of medium. *A*, electron micrographs of EV-enriched pellets recovered by precipitation and by ultracentrifugation from medium conditioned by macrophages treated with 50 ng/ml LPS for 1 h. *Scale bar*, 100 nm. *B*, qRT-PCR analyses of material recovered by enrichment of exosomes from medium, reported relative to *C. elegans* miR39 spike-in. *C*, immunoblot analysis of EV enriched fraction from 2×10^6 cells and whole-cell lysate (5×10^4 cells). Results are mean $\pm$ S.E. (*error bars*) for $n = 3$. *, $p < 0.05$ using ANOVA with Dunnett's multiple-comparison test.

hepatocytes divide approximately once in 150 days in the adult mouse (36), and therefore new rRNA synthesis and 2′-*O*-methylation are expected to occur at much slower rates. Compared with KO mice that had not undergone parabiosis, enterocytes of KO parabionts showed a significant decrease in amplification (relative quantification; RQ), indicating an increase in modification of all four *Rpl13a* snoRNA target sites (lower RQ) and phenocopying the WT parabiont and WT animal control (Fig. 12*A*). By contrast, in liver tissue, we observed no significant difference in modification (RQ) at target sites for U32a and U33 between KO controls and KO parabionts, despite a clear difference between KO controls and either WT controls or WT paraboints (Fig. 12*B*). Unexpectedly, there was no difference between WT and KO controls in apparent methylation in liver tissue at the U34 or U35a snoRNA target sites, raising the possibility that these target sites are unmodified in WT livers or that other snoRNAs could be up-regulated specifically in the KO livers to compensate for the loss of the *Rpl13a* snoRNAs. Importantly, GFP expression remained undetectable in the KO parabiont (Fig. 12, *C* and *D*), indicating the lack of transfer of cellular material. Taken together, our data provide evidence that *Rpl13a* snoRNAs travel through the circulation and are

taken up by distant tissues in which they function to modify their established RNA targets.

Discussion

Herein, we demonstrate that cultured macrophages secrete *Rpl13a* snoRNAs in response to the inflammatory stimulus LPS, most likely as cargo inside of EVs. Furthermore, we show that LPS stimulates secretion of these snoRNAs in both mouse models and in human subjects. By leveraging a recently generated mouse model with selective loss of the *Rpl13a* snoRNAs, we show that these extracellular noncoding RNAs are taken up by cultured macrophages, in which they traffic to the nucleus. In parabiosis experiments, we demonstrate that these snoRNAs are not simply inert passengers in EVs, but are also capable of functioning in distant tissues. Together, our findings provide a new understanding of the biology of snoRNAs and the repertoire of EVs.

EVs secreted from macrophages and other cell types can carry not only membrane and protein components from their cells of origin, but also RNAs that can be detected by sensitive PCR or RNA-Seq–based methods from concentrated preparations of EVs. Microarray and RNA-Seq analyses have provided

⅀ASBMB

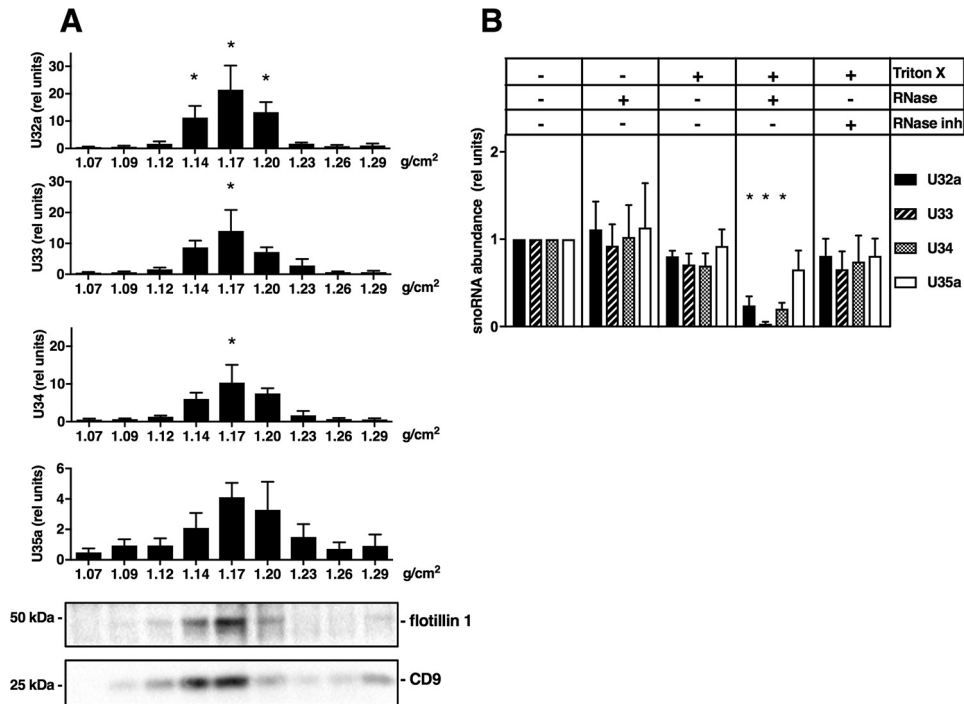*J. Biol. Chem.* (2018) 293(34) 13284–13296 **13289**

Figure 6. Rpl13a snoRNAs are contained within secreted EVs. *A*, qRT-PCR for snoRNAs (relative to *C. elegans* miR39 spike-in) and Western blotting of fractions collected from a continuous sucrose gradient (0.25–2 M) after floating EVs enriched by differential centrifugation from overnight macrophage culture (1.6×10^7 cells). *B*, qRT-PCR of snoRNAs from EV-enriched fraction treated with RNase, Triton X-100, and RNase inhibitor (*Inh*) as indicated. Results are mean ± S.E. (*error bars*) for $n = 3$. *, $p < 0.05$ using ANOVA with Dunnett's multiple-comparison test.
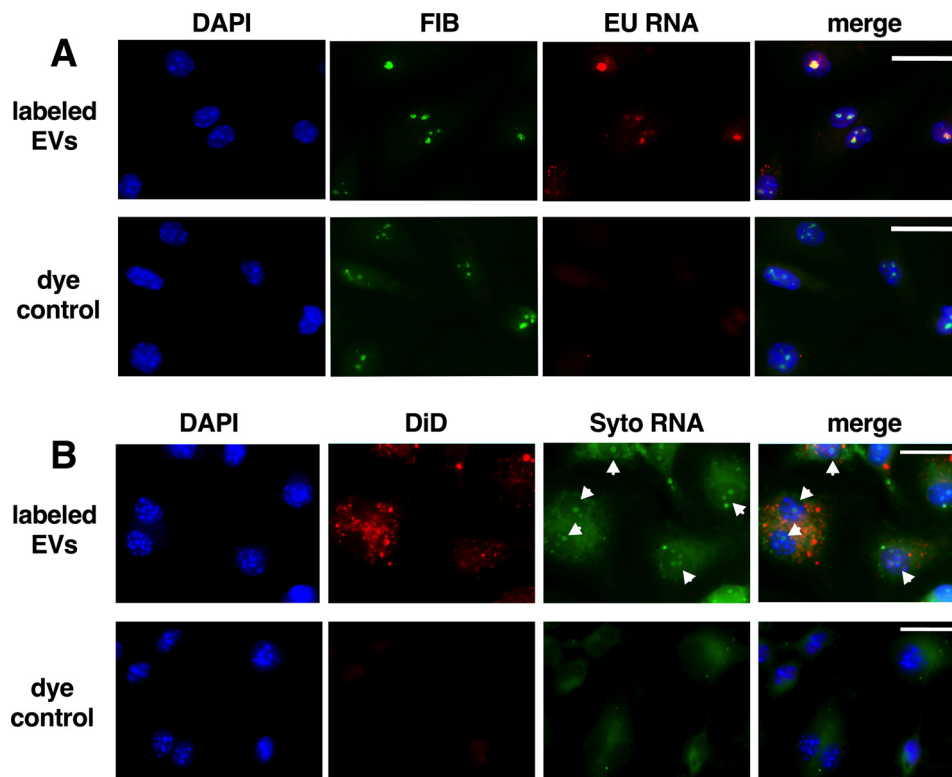

Figure 7. EV tRNA. *A*, WT cells cultured with EVs from ethynyl uridine–labeled WT cells (*EU RNA*), fixed and stained for labeled RNA with Alexa Fluor 594 azide and α-fibrillarin (*FIB*) antibody. Nuclei were counterstained with 4',6-diamidino-2-phenylindole (*DAPI*). Dye control used EVs from cells not labeled with ethynyl uridine. *Scale bar*, 20 μm. *B*, representative images of WT cells cultured with DiD– and Syto RNAselect–labeled WT EVs and fixed and stained with 4',6-diamidino-2-phenylindole. *Scale bar*, 20 μm. Images are representative of three independent experiments.
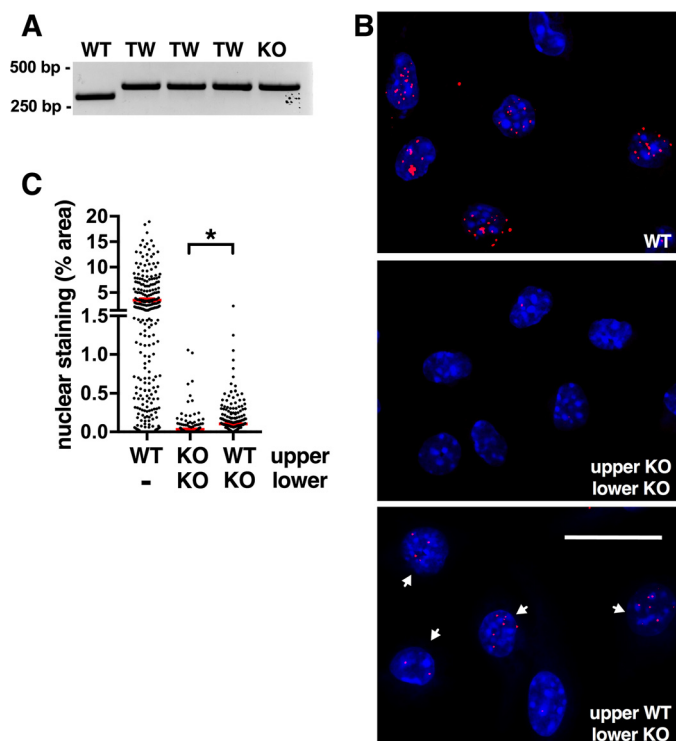
Figure 8. EVs transfer snoRNAs. *A*, representative agarose gel of genotyping PCR on DNA recovered from cells in the lower chamber of a transwell culture plate. *WT*, WT cells in both upper and lower chambers. *TW*, WT cells in the upper chamber and KO cells in the lower chamber. *KO*, KO cells in both upper and lower chambers. *B*, *in situ* Alexa Fluor 546 labeling for U33 in KO cells (lower chamber) that were co-cultured in a transwell apparatus with WT cells or with KO cells (upper chamber). WT cells cultured alone are shown as controls. Representative confocal micrographs are shown. *C*, quantification of 8–9 random fields for each of three independent experiments, with an average of 281 cells/condition. *Scale bars*, 20 μm. Results are mean ± S.E. (*error bars*). *, $p < 0.05$ using Student's *t* test.

Figure 9. LPS stimulates snoRNA secretion *in vivo*. *A* and *B*, mice were treated with 10 mg/kg LPS (*n* = 18) or saline as control (PBS, *n* = 12). At 4 h after treatment, TNFα expression (relative to *Rplp0*) in liver tissue (*A*) and *Rpl13a* snoRNA abundance (relative to spike-in) in serum EVs (*B*) were quantified by qRT-PCR. *C* and *D*, blood was analyzed from human subjects at time 0 (*pre*) and 6 h following (*post*) endobronchial installation of 4 ng/kg LPS. Blood markers of inflammation, C-reactive protein (*CRP*), white blood cell count (*WBC*), and percentage of polymorphonuclear leukocytes (*PMN*) were quantified (*C*). Abundance of *Rpl13a* snoRNA levels in serum EVs (relative to spike-in) was quantified by qRT-PCR (*D*). *n* = 6 subjects. Results are mean ± S.E. (*error bars*); *, $p < 0.05$.

evidence that in addition to mRNAs, long noncoding RNAs, and microRNAs, a range of snoRNA species are present in EVs secreted from cultured cells and in EVs isolated from human blood (17–19, 21, 37). Our work extends these observations by demonstrating that macrophage secretion of EV-associated *Rpl13a* snoRNAs is stimulated by LPS, which is also known to regulate secretion of microRNAs from macrophages (15). Furthermore, we show that the *Rpl13a* snoRNAs are also secreted in response to this inflammatory stimulus in mice and in humans. For our *in vivo* analyses, we enriched for circulating EVs by precipitation from serum samples. Whereas it is possible that serum EVs containing *Rpl13a* snoRNAs originate from macrophages, these snoRNAs are widely expressed, and snoRNA-containing EVs probably originate from additional cell types *in vivo*.

Secretion of snoRNAs *in vivo* raises the possibility that these RNAs traffic in a paracrine or endocrine fashion between cells to impact the biology of recipient cells and to regulate organismal physiology, as has been demonstrated for microRNAs (16). *In vitro*, we used RNA labeling to show that concentrated EVs from donor cells are taken up by recipient cells. We also leveraged primary macrophages from mice with loss of function of the *Rpl13a* snoRNAs and from WT mice to demonstrate that EV-associated snoRNAs are taken up by recipient cells and traffic to the nucleus. Although we detected the presence of trans-
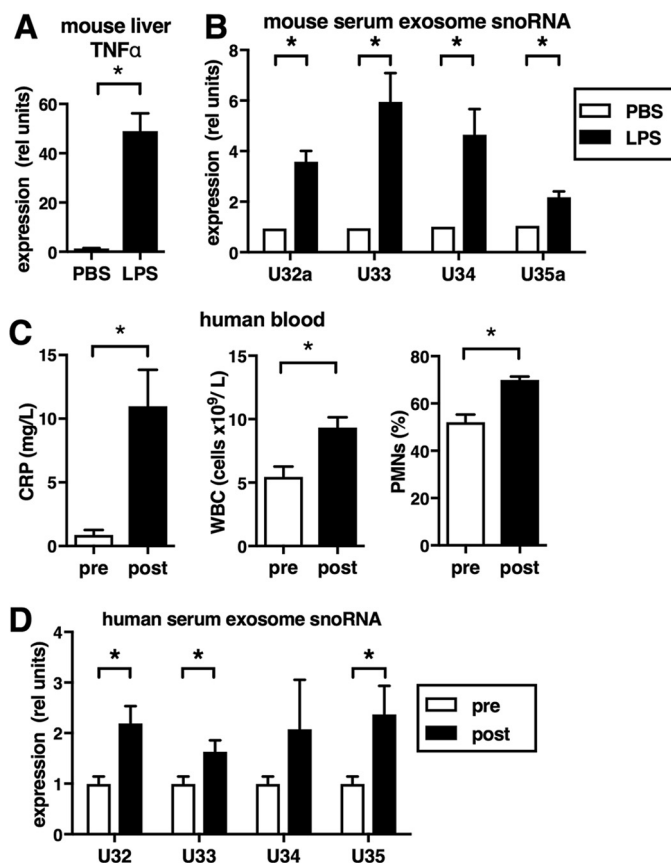
ferred EV RNA and transferred U33 snoRNA, we were unable to consistently detect new 2′-O-methylation in cultured recipient cells treated with concentrated EVs or in co-cultured macrophages. We hypothesize that this is because snoRNAs direct 2′-O-methyl modifications of newly transcribed pre-rRNAs in the nucleolus, but not mature rRNAs (34). Transcription of new rRNA is linked to progression through the cell cycle, which is extremely slow in these nonreplicating primary macrophages (33).

By contrast, in the parabiosis model using WT and KO mice, we find that *Rpl13a* snoRNAs are transferred through the bloodstream and can function in distant tissues, in a setting that does not involve concentration of large quantities of biological fluids. Two features of this model probably facilitated detection of functional snoRNA transfer. First, although the mice were not treated with LPS, sterile inflammation secondary to the surgical procedure may have contributed to EV secretion. Second, our data indicate that shared circulation is established early. Because synthesis of new rRNAs is low in post-mitotic cells and tissues, chronic exposure to snoRNA-containing EVs over several weeks may have enabled detection of snoRNA
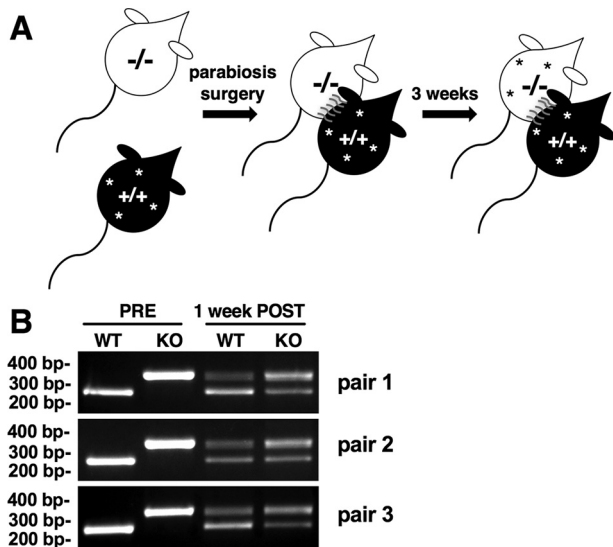
Figure 10. Parabiosis model establishes shared circulation. *A,* parabiosis surgery was performed to join the circulations of WT (+/+) and KO (−/−) mice. The WT mice express GFP (*) in all tissues. Following parabiosis, the presence of GFP in blood stream of both parabionts indicates shared circulation. Analyses for snoRNA transfer to parenchymal tissues of KO parabiont were performed 3 weeks after surgery following perfusion to remove blood. *B,* representative agarose gel of genotyping PCR on DNA recovered from blood collected before and 1 week after surgery from three parabiosis pairs with WT and KO controls.

Figure 11. Detection of *Rpl13a* snoRNA function. *A, schematic* for primer extension qRT-PCR for detection of 2′-*O*-methylation (*2′-O-ME*). Under standard dNTP concentrations, cDNA synthesis proceeds regardless of template RNA methylation (*red cross*). At low, but not high, dNTP concentrations, reverse transcriptase stalls at the methylation site and falls off the template. Concentration of dNTP has no effect on unmethylated RNA template. Thus, the ratio of qRT-PCR efficiency under low/high dNTP (RQ) inversely correlates with methylation at the site of interest. *B,* primer extension qRT-PCR for known rRNA target sites for *Rpl13a* snoRNAs in WT and KO macrophages (18S, G1328 for U32a; 18S, U1326 for U33; 28S, U2590 for U34; 28S, C4188 for U35a). Low RQ indicates more 2′-*O*-methylation. High RQ indicates less/no 2′-*O*-methylation. Results are mean ± S.E. (*error bars*); $n = 3$; *, $p < 0.05$ using Student's *t* test.

function in rapidly replicating enterocytes, which must synthesize and 2′-*O*-methylate new rRNAs. Although our studies demonstrate acquisition of new snoRNA-directed modifications, we were unable to consistently detect *Rpl13a* snoRNAs by qRT-PCR in KO parabiont tissues (not shown). This suggests that snoRNAs are short-lived in recipient tissues relative to the RNA marks they generate and/or that a relatively small number of transferred snoRNA molecules catalyze a substantially larger number of methylation events.

Macrophages play key roles in the response to infection or tissue damage through their activation, polarization, and communication with the extracellular environment. Although it has long been appreciated that the secreted protein cytokines are key mediators of communication between macrophages and distant tissues, evidence is emerging that macrophage-secreted EVs play important roles in pathophysiological responses to inflammation. In the setting of infections with the intracellular pathogens *Mycobacteria* and *Listeria*, macrophages secrete EVs that promote inflammatory signaling, cell migration, and protective T cell–mediated immune responses *in vivo* (38–40). Macrophage-derived EVs have also been shown to play a critical role in the regenerative response of intestinal stem cells following radiation injury (41). In some instances, these functions have been associated with EV transfer of protein antigens (39) or signaling molecules (41). Thus, macrophage EVs have been implicated to serve as immunoregulators. Our data show that macrophage-derived EVs contain snoRNAs that are known to target rRNAs for 2′-*O*-methylation, suggesting that the functional repertoire of macrophage EVs may include broader processes for cellular homeostasis, such as protein expression or cellular growth.

Future studies will be required to elucidate the spectrum of signals that regulate snoRNA secretion, the mechanisms for
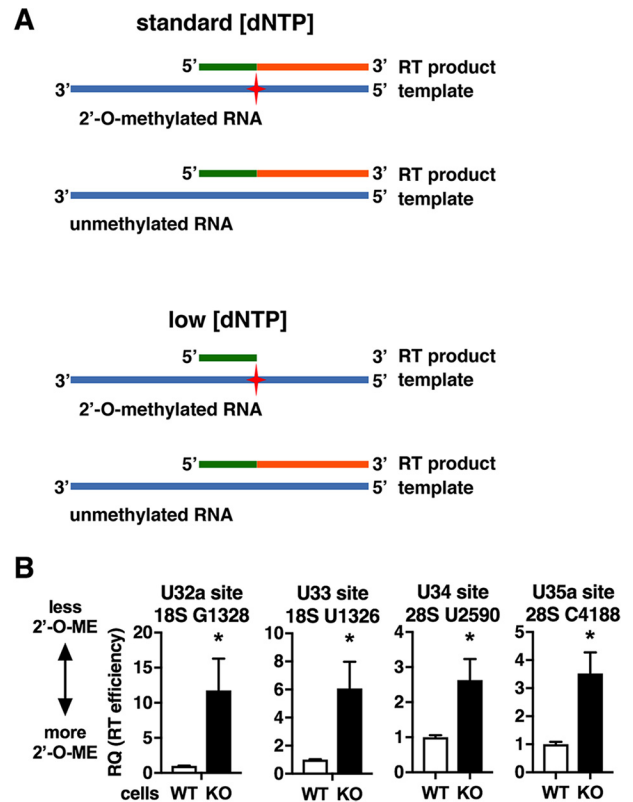
selection of snoRNAs as EV cargo, and whether specific subclasses of EVs carry snoRNAs. The rapidity of release of EVs containing snoRNAs following treatment with ionomycin or LPS suggests that these stimuli promote release of preformed snoRNA-containing EVs. Although secreted snoRNAs that direct rRNA modifications in recipient cells may mediate cell–cell communication, the physiological role of snoRNA secretion remains to be determined. The finding of augmented mitochondrial proton leak in tissues of the *Rpl13a*-snoRNA KO mouse suggests that a noncanonical function of the snoRNAs is to promote tightly coupled respiration (28). Based on this, we hypothesize that EV-mediated snoRNA transfer could enhance metabolic efficiency in recipient cells, thereby improving cell survival in the face of stress and/or infection. Characterization of the physiological contexts that precipitate secretion of snoRNAs could reveal opportunities in which the *Rpl13a* snoRNAs or other snoRNAs might serve as biomarkers for detection or management of disease. Given that snoRNAs are sensitive to antisense knockdown, these noncoding RNAs have the potential to serve as targets for new therapeutic approaches.
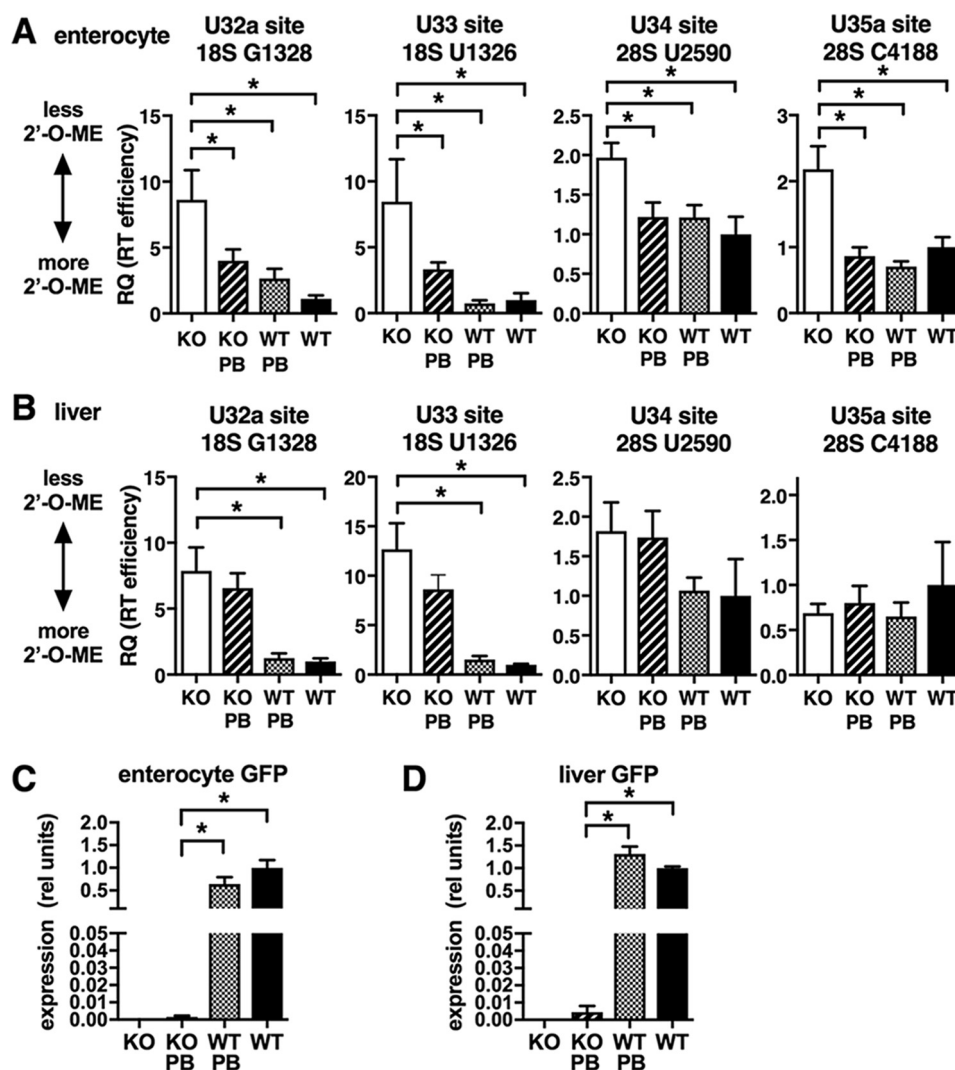
Figure 12. Secreted snoRNAs direct new 2′-O-methylation *in vivo*. Enterocytes (*A* and *C*) and liver tissue (*B* and *D*) were isolated from KO and WT parabionts (*PB*; $n = 10$ each genotype) and from unpaired KO ($n = 5$) and WT ($n = 3$) controls. *A* and *B*, primer extension qRT-PCR for detection of 2′-O-methylation of rRNA targets for *Rpl13a* snoRNAs (18S, G1328 for U32a; 18S, U1326 for U33; 28S, U2590 for U34; 28S, C4188 for U35a). *C* and *D*, qRT-PCR analysis for detection of GFP expression. Results are mean ± S.E. (*error bars*); *, $p < 0.05$ by ANOVA with Dunnett's multiple-comparison test.

Experimental procedures

Reagents

LPS, BFA, IO, CD, and staurosporine were from Sigma-Aldrich. α-Fibrillarin (ab4566), α-nucleophosmin (ab15440), α-flotillin 1 (ab50673), and α-calnexin (ab22595) antibodies were from Abcam (Cambridge, MA). α-Histone H3 (catalog no. 9717) antibody was from Cell Signaling (Danvers, MA). α-CD9 (catalog no. 564236) was from BD Biosciences.

Mice

FVB and FVB.Cg-Tg(CAG-EGFP)B5Nagy/J were obtained from the Jackson Laboratory (Bar Harbor, ME), and *Rpl13a*-snoless (KO) mice (28) were maintained in facilities under specific pathogen-free conditions at Washington University (St. Louis, MO). Bone marrow was isolated as described below. Blood samples were obtained from male and female mice 4 h following intraperitoneal injection of 10 mg/kg LPS. All experimental procedures were approved by the Washington University Animal Studies Committee and were conducted in accordance with the United States Department of Agriculture Animal Welfare Act and the Public Health Service Policy for the Humane Care and Use of Laboratory Animals.

Bone marrow–derived macrophages

Bone marrow was harvested from the tibia and femur of male and female mice. Cells were seeded and differentiated for 6 days in 10% CMG14.12 conditioned medium (42). CMG14.12 cells were a gift from the laboratory of Deborah Veis (Washington University). Cells were treated with 50 ng/ml LPS for the indicated times, 10 μg/ml BFA for 90 min, 0.5 μM IO for 15 min, or 2% CD for 60 min. Cell death was measured using the Cytotox96 nonradioactive cytotoxicity assay (Promega, Madison, WI). LDH$^+$ controls contained LDH from the kit (1:5,000 dilution of 1,600 units/ml solution), and the maximum signal was determined by measuring LDH activity in the medium of cells cultured under identical conditions and lysed by quickly freezing and thawing the plate. Apoptosis was quantified by a caspase 3/7 Glo assay (Promega, Madison, WI). ROS was

detected by measuring fluorescence on a TECAN Infinite 200 PRO multimode reader (Tecan, Männedorf, Switzerland) after cells were loaded with 10 μM DCF (Thermo Fisher Scientific, Carlsbad, CA). Sequential detergent extraction was performed as described previously to generate nuclear and cytosolic fractions (10).

EV enrichment, labeling, and transfer

EVs were isolated from cell culture medium using Total Exosome isolation reagent (Thermo Fisher Scientific) (43), or EVs were isolated by differential centrifugation (44). Serum EVs were isolated with Exoquick (System Biosciences, Mountain View, CA) according to the manufacturer's instructions (38). Culture medium used for EV labeling/transfer and floatation/ RNase treatment experiments was depleted of EVs before use by centrifugation at $120,000 \times g$ for 90 min. Conditioned medium was cleared by centrifugation for 10 min at $1,000 \times g$, followed by centrifugation for 20 min at $2,000 \times g$, and then concentrated using an Amicon Ultra-15 centrifugal filter unit with Ultracel-10 membrane ($3,500 \times g$, 20 min; Millipore, Billerica, MA). EVs were floated into a continuous sucrose gradient as described previously (44). A small sample was taken from each fraction, and density was measured at room temperature using an Atago (Bellevue, WA) three-range sugar hand refractometer (0–90%).

For EV transfer experiments, EVs were labeled using Syto RNA select and DiD (Thermo Fisher Scientific) according to the manufacturer's instructions, and unincorporated dye was removed either by washing in Amicon filters or with Exosome spin columns (Thermo Fisher Scientific) with similar results. Dye controls were treated in an identical manner. Ethynyl uridine–labeled EVs were collected from cells cultured overnight with 0.5 mM ethynyl uridine (45). Following incubation of recipient cells with EVs for 45 min, cells were washed twice with 3% BSA (Sigma-Aldrich) in PBS, fixed with 3.7% paraformaldehyde, (Electron Microscopy Science, Hatfield, PA), and permeabilized with 0.5% Triton X-100 (Sigma-Aldrich). Ethynyl uridine was detected using the Click iT RNA imaging kit (Alexa Fluor 594, Thermo Fisher Scientific). For transwell transfer, 10^6 KO and WT bone marrow cells were grown for 7 days or until confluent in conditioned medium in chambers separated by Thincert 1-μm pore membranes (Greiner Bio-one) in 6-well plates and stained using the Quantigene ViewRNA Cell Plus assay with Alexa Fluor 546 detection, modified to include an additional fixation with 1-ethyl-3-(3-dimethylaminopropyl) carbodiimide hydrochloride and protease treatment with reagents from the miRNA assay kit. Control wells were assayed for transfer of genomic material using genotyping primers for WT and KO *Rpl13a* loci (28).

qRT-PCR

RNA was purified using TRIzol. Relative quantification of RNA abundance was calculated using the $\Delta\Delta Ct$ method on an ABI 7500 fast real-time PCR system. Primer sequences for *COX2* were TGA GCA ACT ATT CCA AAC CAG C (forward) and GCA CGT AGT CTT CGA TCA CTA TC (reverse); for *TNFα*, they were CAT CTT CTC AAA ATT CGA GTG ACA A (forward) and TGG GAG TAG ACA AGG TAC AAC CC

(reverse); and for *Rplp0*, they were ATC CCT GAC GCA CCG CCG TGA (forward) and TGC ATC TGC TTG GAG CCC ACG TT (reverse). The method for qRT-PCR for *Rpl13a* snoRNAs used target-specific stem loop RT primers, a target-specific forward PCR primer, and a universal reverse PCR primer (46). This method can detect as few as 10^3 copies of target RNAs, is able to distinguish between small RNA species that differ by only 1 nucleotide, is not affected by genomic contamination, distinguishes mature snoRNAs and miRNAs from their precursor small RNA species, and has been validated against RNA-Seq for snoRNAs (10, 47, 48). mRNA quantification was calculated using *Rplp0* as an endogenous control. For quantification of EV RNA, *Caenorhabditis elegans* miR39 (500 fmol) or luciferase mRNA (0.3 fmol; Promega) was added to EV samples before RNA isolation and used as a reference control. Amplification of reference genes varied by <1 cycle across samples. A plate of 2×10^6 cells was used for cellular fractionation by sequential detergent extraction, and medium was pooled from three plates.

Microscopy

Freeze fracture/deep etch EM was performed according to published protocols with minor modifications (49). A 4-μl droplet of sample was placed on top of a 4×4-mm acid-cleaned and air-dried coverslip and then topped with a 3-mm round sapphire disc. Samples were immediately frozen by abrupt application of the sample against a liquid helium–cooled copper block with a Cryopress freezing machine. Frozen samples were transferred to a liquid nitrogen–cooled Balzers 400 vacuum evaporator, fractured at -100 °C by removal of the sapphire disc with the instrument's nitrogen cooled knife. Samples were etched for 2 min at -100 °C and rotary replicated with ~2-nm platinum deposited from a 20º angle above the horizontal, followed by an immediate ~4-nm stabilization film of pure carbon deposited from an 85º angle. Replicas were floated onto a dish of concentrated hydrofluoric acid for coverslip removal and then transferred through several rinses of distilled H_2O with a loopful of Photoflo, picked up on Formvar-coated grids, and photographed on a JEOL 1400 microscope with attached AMT digital camera. Confocal images were taken on a Zeiss LSM 880 Airyscan confocal microscope with a 0.8-μm pinhole through a focal plane in the center of the nuclei and processed using Zen software (Zeiss, Oberkochen, Germany).

RNase protection

EVs enriched by ultracentrifugation were suspended in 250 μl of PBS and treated with 0.3% Triton X-100, 1 unit of RNase A, 40 units of RNase T1 (Ambion RNase mixture, Thermo Fisher Scientific), and 100 units of SUPERase-In RNase inhibitor (Thermo Fisher Scientific) for 30 min at 20 °C, and then RNase inhibitor was added to all samples. RNA was isolated using TRIzol LS.

Human subjects

Blood samples were collected from human volunteers for a study of lung inflammation before and 6 h following endobronchial instillation of 4 ng/kg LPS (29). This study was approved by the Washington University Human Research Protection

Office and complies with the Declaration of Helsinki principles. Informed consent was obtained from all subjects.

Parabiosis

The Washington University Mouse Cardiovascular Phenotyping Core performed parabiosis surgery using female WT mice expressing GFP and *Rpl13a* snoRNA KO mice as described (30). Tail vein blood was sampled serially from the parabionts for PCR analysis of DNA to detect the WT and KO *Rpl13a* loci with primers GAC AGG TTG CTG CTC AGG AAG TAA ATGG (forward) and CCA GAC CTG CTT TCA GAC TTT AGC CTG (reverse). Three weeks following surgery, parabionts were perfused with PBS to clear blood from tissues and euthanized. Enterocytes and liver were recovered and flash-frozen in liquid nitrogen. For PCR analysis, tissues were homogenized in TRIzol.

Primer extension qRT-PCR

Primer extension PCR to detect rRNA methylation was adapted from Dong *et al.* (31). For each target, 20 ng of total RNA was used in cDNA synthesis using the Super Script III kit (Thermo Fisher Scientific) with 0.3 μl of SSIII enzyme per reaction and dNTP at either the normal stock concentration (50 μM) or diluted 1:1,000 (50 nM). The following primers were used for each RT reaction: m18S RT (U32a, G1328), CAA CTA AGA ACG GCC ATG CA; m18S RT (U33, U1326), AGA ACG GCC ATG CAC C; m28S RT (U34, U2590), GAC TTC CCT TAC CTA C; and m28S RT (U35a, C4188), AAC CTG TCT CAC GAC G. qPCR was done on a 7500 fast real-time PCR system with SYBR Green real-time PCR master mix (Thermo Fisher Scientific). PCR primers used were as follows: m18S F2 (U32a/33), GGC CTG CGG CTT AAT TTG AC; m18S R2 (U32/33), ATG CAC CAC CAC CCA CG; m28S F1 (U34), TCT CGC TGG CCC TTG AAA AT; m28S R1 (U34), ACC TAC ATT GTT CCA ACA TGC C; m28S F1 (U35a), CTT CGA TGT CGG CTC TTC CT; m28S R1 (U35a), TCA CGA CGG TCT AAA CCC AG. RT efficiency was calculated by normalizing the *Ct* value for the low dNTP concentration to the high as an endogenous control (RQ). For each modification site within a specific tissue, values are reported relative to the mean WT value.

References

1. Bachellerie, J. P., Cavaillé, J., and Hüttenhofer, A. (2002) The expanding snoRNA world. *Biochimie* **84,** 775–790 CrossRef Medline
2. Dupuis-Sandoval, F., Poirier, M., and Scott, M. S. (2015) The emerging landscape of small nucleolar RNAs in cell biology. *Wiley Interdiscip. Rev. RNA* **6,** 381–397 CrossRef Medline
3. Kiss, T., Fayet, E., Jády, B. E., Richard, P., and Weber, M. (2006) Biogenesis and intranuclear trafficking of human box C/D and H/ACA RNPs. *Cold Spring Harb. Symp. Quant. Biol.* **71,** 407–417 CrossRef Medline
4. Terns, M. P., and Terns, R. M. (2002) Small nucleolar RNAs: versatile trans-acting molecules of ancient evolutionary origin. *Gene. Expr.* **10,** 17–39 Medline
5. Watkins, N. J., Lemm, I., Ingelfinger, D., Schneider, C., Hossbach, M., Urlaub, H., and Lührmann, R. (2004) Assembly and maturation of the U3 snoRNP in the nucleoplasm in a large dynamic multiprotein complex. *Mol. Cell* **16,** 789–798 CrossRef Medline
6. Baserga, S. J., Gilmore-Hebert, M., and Yang, X. W. (1992) Distinct molecular signals for nuclear import of the nucleolar snRNA, U3. *Genes Dev.* **6,** 1120–1130 CrossRef Medline
7. Watkins, N. J., Lemm, I., and Lührmann, R. (2007) Involvement of nuclear import and export factors in U8 box C/D snoRNP biogenesis. *Mol. Cell Biol.* **27,** 7018–7027 CrossRef Medline
8. Sienna, N., Larson, D. E., and Sells, B. H. (1996) Altered subcellular distribution of U3 snRNA in response to serum in mouse fibroblasts. *Exp. Cell Res.* **227,** 98–105 CrossRef Medline
9. Michel, C. I., Holley, C. L., Scruggs, B. S., Sidhu, R., Brookheart, R. T., Listenberger, L. L., Behlke, M. A., Ory, D. S., and Schaffer, J. E. (2011) Small nucleolar RNAs U32a, U33, and U35a are critical mediators of metabolic stress. *Cell Metab.* **14,** 33–44 CrossRef Medline
10. Holley, C. L., Li, M. W., Scruggs, B. S., Matkovich, S. J., Ory, D. S., and Schaffer, J. E. (2015) Cytosolic accumulation of small nucleolar RNAs (snoRNAs) is dynamically regulated by NADPH oxidase. *J. Biol. Chem.* **290,** 11741–11748 CrossRef Medline
11. Li, M. W., Sletten, A. C., Lee, J., Pyles, K. D., Matkovich, S. J., Ory, D. S., and Schaffer, J. E. (2017) Nuclear export factor 3 regulates localization of small nucleolar RNAs. *J. Biol. Chem.* **292,** 20228–20239 CrossRef Medline
12. Valadi, H., Ekström, K., Bossios, A., Sjöstrand, M., Lee, J. J., and Lötvall, J. O. (2007) Exosome-mediated transfer of mRNAs and microRNAs is a novel mechanism of genetic exchange between cells. *Nat. Cell Biol.* **9,** 654–659 CrossRef Medline
13. Vickers, K. C., Palmisano, B. T., Shoucri, B. M., Shamburek, R. D., and Remaley, A. T. (2011) MicroRNAs are transported in plasma and delivered to recipient cells by high-density lipoproteins. *Nat. Cell Biol.* **13,** 423–433 CrossRef Medline
14. Cortez, M. A., Bueso-Ramos, C., Ferdin, J., Lopez-Berestein, G., Sood, A. K., and Calin, G. A. (2011) MicroRNAs in body fluids–the mix of hormones and biomarkers. *Nat. Rev. Clin. Oncol.* **8,** 467–477 CrossRef Medline
15. Zhang, Y., Liu, D., Chen, X., Li, J., Li, L., Bian, Z., Sun, F., Lu, J., Yin, Y., Cai, X., Sun, Q., Wang, K., Ba, Y., Wang, Q., Wang, D., *et al.* (2010) Secreted monocytic miR-150 enhances targeted endothelial cell migration. *Mol. Cell* **39,** 133–144 CrossRef Medline
16. Ying, W., Riopel, M., Bandyopadhyay, G., Dong, Y., Birmingham, A., Seo, J. B., Ofrecio, J. M., Wollam, J., Hernandez-Carretero, A., Fu, W., Li, P., and Olefsky, J. M. (2017) Adipose tissue macrophage-derived exosomal miRNAs can modulate *in vivo* and *in vitro* insulin sensitivity. *Cell* **171,** 372–384.e12 CrossRef Medline
17. Lefebvre, F. A., Benoit Bouvrette, L. P., Perras, L., Blanchet-Cohen, A., Garnier, D., Rak, J., and Lécuyer, É. (2016) Comparative transcriptomic analysis of human and *Drosophila* extracellular vesicles. *Sci. Rep.* **6,** 27680 CrossRef Medline
18. Kaur, S., Elkahloun, A. G., Arakelyan, A., Young, L., Myers, T. G., Otaizo-Carrasquero, F., Wu, W., Margolis, L., and Roberts, D. D. (2018) CD63, MHC class 1, and CD47 identify subsets of extracellular vesicles containing distinct populations of noncoding RNAs. *Sci. Rep.* **8,** 2577 CrossRef Medline

19. Wei, Z., Batagov, A. O., Schinelli, S., Wang, J., Wang, Y., El Fatimy, R., Rabinovsky, R., Balaj, L., Chen, C. C., Hochberg, F., Carter, B., Breakefield, X. O., and Krichevsky, A. M. (2017) Coding and noncoding landscape of extracellular RNA released by human glioma stem cells. *Nat. Commun.* **8,** 1145 CrossRef Medline

20. Valleron, W., Ysebaert, L., Berquet, L., Fataccioli, V., Quelen, C., Martin, A., Parrens, M., Lamant, L., de Leval, L., Gisselbrecht, C., Gaulard, P., and Brousset, P. (2012) Small nucleolar RNA expression profiling identifies potential prognostic markers in peripheral T-cell lymphoma. *Blood* **120,** 3997–4005 CrossRef Medline

21. Huang, X., Yuan, T., Tschannen, M., Sun, Z., Jacob, H., Du, M., Liang, M., Dittmar, R. L., Liu, Y., Liang, M., Kohli, M., Thibodeau, S. N., Boardman, L., and Wang, L. (2013) Characterization of human plasma-derived exosomal RNAs by deep sequencing. *BMC Genomics* **14,** 319 CrossRef Medline

22. Scruggs, B. S., Michel, C. I., Ory, D. S., and Schaffer, J. E. (2012) SmD3 regulates intronic noncoding RNA biogenesis. *Mol. Cell Biol.* **32,** 4092–4103 CrossRef Medline

23. Shi, M. M., Chong, I., Godleski, J. J., and Paulauskis, J. D. (1999) Regulation of macrophage inflammatory protein-2 gene expression by oxidative stress in rat alveolar macrophages. *Immunology* **97,** 309–315 CrossRef Medline

24. Simons, M., and Raposo, G. (2009) Exosomes–vesicular carriers for intercellular communication. *Curr. Opin. Cell Biol.* **21,** 575–581 CrossRef Medline

25. Savina, A., Furlán, M., Vidal, M., and Colombo, M. I. (2003) Exosome release is regulated by a calcium-dependent mechanism in K562 cells. *J. Biol. Chem.* **278,** 20083–20090 CrossRef Medline

26. Chen, F. W., Li, C., and Ioannou, Y. A. (2010) Cyclodextrin induces calcium-dependent lysosomal exocytosis. *PLoS One* **5,** e15054 CrossRef Medline

27. Helwa, I., Cai, J., Drewry, M. D., Zimmerman, A., Dinkins, M. B., Khaled, M. L., Seremwe, M., Dismuke, W. M., Bieberich, E., Stamer, W. D., Hamrick, M. W., and Liu, Y. (2017) A comparative study of serum exosome isolation using differential ultracentrifugation and three commercial reagents. *PLoS One* **12,** e0170628 CrossRef Medline

28. Lee, J., Harris, A. N., Holley, C. L., Mahadevan, J., Pyles, K. D., Lavagnino, Z., Scherrer, D. E., Fujiwara, H., Sidhu, R., Zhang, J., Huang, S. C. C., Piston, D. W., Remedi, M. S., Urano, F., Ory, D. S., and Schaffer, J. E. (2016) Rpl13a small nucleolar RNAs regulate systemic glucose metabolism. *J. Clin. Invest.* **126,** 4616–4625 CrossRef Medline

29. Chen, D. L., Huang, H. J., Byers, D. E., Shifren, A., Belikoff, B., Engle, J. T., Arentson, E., Kemp, D., Phillips, S., Scherrer, D. E., Fujiwara, H., Spayd, K. J., Brooks, F. J., Pierce, R. A., Castro, M., and Isakow, W. (2018) The peroxisome proliferator-activated receptor agonist pioglitazone and 5-lipoxygenase inhibitor zileuton have no effect on lung inflammation in healthy volunteers by positron emission tomography in a single-blind placebo-controlled cohort study. *PLoS One* **13,** e0191783 CrossRef Medline

30. Kamran, P., Sereti, K. I., Zhao, P., Ali, S. R., Weissman, I. L., and Ardehali, R. (2013) Parabiosis in mice: a detailed protocol. *J. Vis. Exp.* CrossRef Medline

31. Dong, Z. W., Shao, P., Diao, L. T., Zhou, H., Yu, C. H., and Qu, L. H. (2012) RTL-P: a sensitive approach for detecting sites of 2′-*O*-methylation in RNA molecules. *Nucleic Acids Res.* **40,** e157 CrossRef Medline

32. Brandis, K. A., Gale, S., Jinn, S., Langmade, S. J., Dudley-Rucker, N., Jiang, H., Sidhu, R., Ren, A., Goldberg, A., Schaffer, J. E., and Ory, D. S. (2013) Box C/D small nucleolar RNA (snoRNA) U60 regulates intracellular cholesterol trafficking. *J. Biol. Chem.* **288,** 35703–35713 CrossRef Medline

33. Grummt, I. (2003) Life on a planet of its own: regulation of RNA polymerase I transcription in the nucleolus. *Genes Dev.* **17,** 1691–1702 CrossRef Medline

34. Kos, M., and Tollervey, D. (2010) Yeast pre-rRNA processing and modification occur cotranscriptionally. *Mol. Cell* **37,** 809–820 CrossRef Medline

35. Darwich, A. S., Aslam, U., Ashcroft, D. M., and Rostami-Hodjegan, A. (2014) Meta-analysis of the turnover of intestinal epithelia in preclinical animal species and humans. *Drug Metab. Dispos.* **42,** 2016–2022 CrossRef Medline

36. Magami, Y., Azuma, T., Inokuchi, H., Kokuno, S., Moriyasu, F., Kawai, K., and Hattori, T. (2002) Cell proliferation and renewal of normal hepatocytes and bile duct cells in adult mouse liver. *Liver* **22,** 419–425 CrossRef Medline

37. Berardocco, M., Radeghieri, A., Busatto, S., Gallorini, M., Raggi, C., Gissi, C., D'Agnano, I., Bergese, P., Felsani, A., and Berardi, A. C. (2017) RNA-seq reveals distinctive RNA profiles of small extracellular vesicles from different human liver cancer cell lines. *Oncotarget* **8,** 82920–82939 Medline

38. Singh, P. P., Smith, V. L., Karakousis, P. C., and Schorey, J. S. (2012) Exosomes isolated from mycobacteria-infected mice or cultured macrophages can recruit and activate immune cells *in vitro* and *in vivo*. *J. Immunol.* **189,** 777–785 CrossRef Medline

39. Zhang, Y., Zhang, R., Zhang, H., Liu, J., Yang, Z., Xu, P., Cai, W., Lu, G., Cui, M., Schwendener, R. A., Shi, H. Z., Xiong, H., and Huang, B. (2012) Microparticles released by *Listeria monocytogenes*-infected macrophages are required for dendritic cell-elicited protective immunity. *Cell Mol. Immunol.* **9,** 489–496 CrossRef Medline

40. Walters, S. B., Kieckbusch, J., Nagalingam, G., Swain, A., Latham, S. L., Grau, G. E., Britton, W. J., Combes, V., and Saunders, B. M. (2013) Microparticles from mycobacteria-infected macrophages promote inflammation and cellular migration. *J. Immunol.* **190,** 669–677 CrossRef Medline

41. Saha, S., Aranda, E., Hayakawa, Y., Bhanja, P., Atay, S., Brodin, N. P., Li, J., Asfaha, S., Liu, L., Tailor, Y., Zhang, J., Godwin, A. K., Tome, W. A., Wang, T. C., Guha, C., and Pollard, J. W. (2016) Macrophage-derived extracellular vesicle-packaged WNTs rescue intestinal stem cells and enhance survival after radiation injury. *Nat. Commun.* **7,** 13096 CrossRef Medline

42. Takeshita, S., Kaji, K., and Kudo, A. (2000) Identification and characterization of the new osteoclast progenitor with macrophage phenotypes being able to differentiate into mature osteoclasts. *J. Bone Miner. Res.* **15,** 1477–1488 CrossRef Medline

43. Lane, R. E., Korbie, D., Anderson, W., Vaidyanathan, R., and Trau, M. (2015) Analysis of exosome purification methods using a model liposome system and tunable-resistive pulse sensing. *Sci. Rep.* **5,** 7639 CrossRef Medline

44. Thery, C., Amigorena, S., Raposo, G., and Clayton, A. (2006) Isolation and characterization of exosomes from cell culture supernatants and biological fluids. *Curr. Protoc. Cell Biol.*, Chapter 3, Unit 3.22 CrossRef Medline

45. Jinn, S., Brandis, K. A., Ren, A., Chacko, A., Dudley-Rucker, N., Gale, S. E., Sidhu, R., Fujiwara, H., Jiang, H., Olsen, B. N., Schaffer, J. E., and Ory, D. S. (2015) snoRNA U17 regulates cellular cholesterol trafficking. *Cell Metab.* **21,** 855–867 CrossRef Medline

46. Feng, J., Wang, K., Liu, X., Chen, S., and Chen, J. (2009) The quantification of tomato microRNAs response to viral infection by stem-loop real-time RT-PCR. *Gene* **437,** 14–21 CrossRef Medline

47. Yang, L. H., Wang, S. L., Tang, L. L., Liu, B., Ye, W. L., Wang, L. L., Wang, Z. Y., Zhou, M. T., and Chen, B. C. (2014) Universal stem-loop primer method for screening and quantification of microRNA. *PLoS One* **9,** e115293 CrossRef Medline

48. Chen, C., Ridzon, D. A., Broomer, A. J., Zhou, Z., Lee, D. H., Nguyen, J. T., Barbisin, M., Xu, N. L., Mahuvakar, V. R., Andersen, M. R., Lao, K. Q., Livak, K. J., and Guegler, K. J. (2005) Real-time quantification of microRNAs by stem-loop RT-PCR. *Nucleic Acids Res.* **33,** e179 CrossRef Medline

49. Heuser, J. (1980) Three-dimensional visualization of coated vesicle formation in fibroblasts. *J. Cell Biol.* **84,** 560–583 CrossRef Medline

ASBMB